Terahertz photovoltaic detection of cyclotron resonance in the regime of radiation-induced magnetoresistance oscillations

R. G. Mani, A. N. Ramanayaka, and Tianyu Ye
Department of Physics and Astronomy, Georgia State University, Atlanta, Georgia 30303, USA

M. S. Heimbeck
Aviation & Missile Research, Development, and Engineering Center (AMRDEC), Redstone Arsenal, Huntsville, Alabama 35898, USA

H. O. Everitt
Aviation & Missile Research, Development, and Engineering Center (AMRDEC), Redstone Arsenal, Huntsville, Alabama 35898, USA and Department of Physics & Departments of Electrical and Computer Engineering, Duke University, Durham, North Carolina 27708-0305, USA

W. Wegscheider
Laboratorium für Festkörperphysik, ETH Zürich, 8093 Zürich, Switzerland

(Received 6 January 2013; revised manuscript received 19 May 2013; published 17 June 2013)

We examine and compare the diagonal magnetoresistance, R_{xx}, and the photovoltage induced by microwave ($42 \leqslant f < 300$ GHz) and terahertz ($f \geqslant 300$ GHz) photoexcitation in the high mobility quasi-two-dimensional GaAs/AlGaAs system. The data demonstrate strong radiation-induced magnetoresistance oscillations in R_{xx} to 360 GHz. In addition, cyclotron resonance is observed in the photovoltage to 725 GHz. These results show that our high-mobility GaAs/AlGaAs two-dimensional electron system (2DES) specimens remain photoactive in magnetotransport into the terahertz band.

DOI: 10.1103/PhysRevB.87.245308 PACS number(s): 72.20.My, 72.20.Fr, 72.80.Ey, 73.43.Fj

I. INTRODUCTION

Microwave photoexcited transport studies of the GaAs/AlGaAs two-dimensional electron system (2DES) at high filling factors or low magnetic fields, B, have revealed new physical effects, such as the radiation-induced zero-resistance states and associated "1/4-cycle shifted" magnetoresistance oscillations.[1] Related phenomena have been the topic of many experimental[1–33] and theoretical[34–62] investigations of transport in the photo-excited 2DES.

The microwave radiation-induced magnetoresistance oscillations in the 2DES are characterized by B^{-1} periodic oscillations in the diagonal magnetoresistance, R_{xx}, of the 2DES at cryogenic temperatures, T, with oscillatory nodes near integral and half-integral multiples of cyclotron resonance.[1,5,32] These R_{xx} oscillations show a nonlinear dependence on the microwave power, P, at modest P,[25,60] and a strong sensitivity to T.[1] Proposed mechanisms for such oscillations include radiation-assisted indirect inter-Landau-level scattering by phonons and impurities (the displacement model),[34,36,39,57] nonparabolicity effects in an ac-driven system (the nonparabolicity model),[38] the periodic motion of the electron orbit centers under irradiation (the radiation driven electron orbit model),[46,49] and a radiation-induced steady state nonequilibrium distribution (the inelastic model).[45] Notably, the last model predicts radiation-polarization insensitivity,[45] while recent experiments and theory have demonstrated a remarkable sensitivity in the amplitude of the radiation-induced magnetoresistance oscillations to the orientation of the linear microwave polarization.[29,30,61,62]

A topic of open interest in this field of radiation-induced transport relates to the responsivity of the 2DES to photoexcitation at radiation frequencies, f, above 100 GHz. Works examining this regime include Refs. 1,15,17–19, and 21–23. Here, Ref. 15 exhibited radiation-induced magnetoresistance oscillations to 254 GHz. Reference 18 is especially remarkable because it reported that the radiation-induced magnetoresistance oscillations begin to quench at 120 GHz and disappear completely above 230 GHz. The quench involved both a decay in the amplitude of the oscillations and a reduction in the number of observable oscillations with increasing radiation frequency. Thus, the authors suggested that the Landau level broadening increased—and the single particle lifetime decreased—rapidly with increasing f, in contradiction to the usual expectation that the broadening is independent of f. Wirthmann *et al.*[19] examined the effect of far-infrared excitation ($\lambda = 184.3$ μm) on a very long GaAs/AlGaAs quantum well meandering Hall bar specimen with mobility $\mu = 1.6 \times 10^6$ cm^2/V s and effective mass $m^*/m = 0.0759$, and reported observing radiation-induced magnetoresistance oscillations in the ΔR_{xx} response to chopped radiation. Tung *et al.* examined long Hall bars and Corbino rings at submillimeter-wave frequencies, and reported a double lock-in photoresistance signal up to 495 GHz.[23] Other experimental work by Mani *et al.*[1,17,21,22] indicated zero-resistance states and radiation-induced magnetoresistance oscillations in R_{xx} above 100 GHz.

Experiments at such high frequencies confront the technological problem of generating radiation at adequate power levels, detecting the radiation, and effectively channeling this radiation to the specimen with minimal losses. In fact, associated practical problems are of sufficient interest that much research and development is devoted to addressing these issues without addressing the end use of high-frequency terahertz radiation.[63–66] Indeed, the terahertz band [0.3 – 10 THz] presents unique challenges because it lies within the frequency span where neither electronic approaches

nor optical techniques function very effectively. Yet, from the applications perspective, detectors and compact radiation sources are needed here for imaging for security and medical applications, bioagent identification, and large-bandwidth communications.[63–66]

Here, we focus upon radiation-induced transport above 200 GHz in the high-mobility GaAs/AlGaAs system using recently developed Schottky diode multiplier chains to boost a high-power, low-frequency signal up to f as large as 780 GHz. A consequence of using multipliers in sources is that the available radiation power drops with increasing frequency and multiplication factor.

The magnetotransport experiments indicate strong radiation-induced magnetoresistance oscillations in the directly measured R_{xx} up to 360 GHz. At higher frequencies, oscillation amplitude drops in part due to inadequate excitation power. A concurrent study of the photovoltage signal indicates, however, continued response up to 725 GHz. The photovoltage response is consistent with cyclotron resonance based on the observed variation of the resonance field, B_R, with f. The results show that our high-mobility 2DES specimens remain microwave and terahertz active up to at least 725 GHz.

II. EXPERIMENT

The GaAs/AlGaAs material utilized for this study was characterized by electron mobility $\mu \approx 10^7$ cm^2/V s and electron density in the range $2.4 \times 10^{11} \leqslant n \leqslant 3 \times 10^{11}$ cm^{-2}. Devices examined here include cleaved specimens with alloyed indium contacts and Hall bars fabricated by optical lithography with alloyed Au-Ge/Ni contacts. The Hall bars were 200 μm wide and the measured sections showed a length-to-width ratio $L/W = 2$.

At lower frequencies, the photoexcitation was generated using commercially available synthesizers with supplementary millimeter wave modules. In the terahertz regime, a highly stable and frequency tunable microwave oscillator in the 10–20 GHz region, with a linewidth of 1 Hz and output power of 17 dBm, excited a series of voltage biased- and unbiased- frequency multipliers. The frequency multiplication stage immediately following the 10–20 GHz oscillator was a frequency-doubling Spacek amplifier. Subsequent frequency multipliers, based on a planar GaAs Schottky diode technology developed by Virginia Diodes, Inc.,[67] have individual multiplication factors of $\times 2$ or $\times 3$ and are daisy-chained to obtain the desired output frequency up to 780 GHz. Over the bands $330 \leqslant f \leqslant 390$ GHz, $430 \leqslant f \leqslant 520$ GHz, and $660 \leqslant f \leqslant 780$ GHz, the source power spanned 2–6 mW, 1–2.5 mW, and 0.3–0.6 mW, respectively. In the THz regime, attenuation between the radiation source and specimen is estimated to be between 10 and 20 dB, caused by a number of factors including mode mismatch, Ohmic losses, and atmospheric attenuation at the highest frequencies.

Electrical measurements of the diagonal resistance, R_{xx}, were carried out by passing a low-frequency ($\approx$13 Hz) current, I, through the specimen via a set of "current" contacts and detecting the voltage drop, V_{xx}, in a four-terminal configuration across a second set of "voltage" contacts using standard low-frequency lock-in techniques. The diagonal resistance is numerically evaluated as $R_{xx} = V_{xx}/I$ after the measurement.

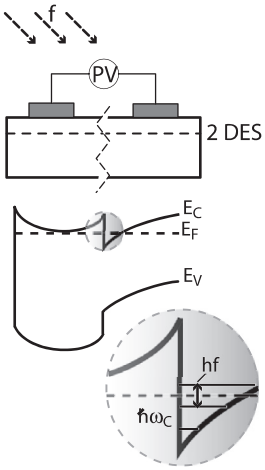

FIG. 1. This figure shows a schematic of the photovoltage experiment. Top: A lock-in amplifier measures the photovoltage (PV) developed between a pair of nominally Ohmic contacts on the surface of the GaAs/AlGaAs device, as the device is photoexcited by chopped microwave and terahertz radiation at frequency f. Here, the 2D electron system (2DES) is located nearly 100 nm below the surface of the semiconductor. Center: This sketch shows the band diagram of the GaAs/AlGaAs heterostructure system, with a Schottky barrier (shown on the left) at the top surface, and a triangular well at the GaAs-AlGaAs interface, which hosts the 2DES. Bottom: An expanded view of the triangular well under the influence of a magnetic field. Here, the triangular well shows Landau levels spaced by $\Delta E = \hbar\omega_c$, and photoexcitation at photon energy hf produces inter-Landau-level transitions.

The PV measurement is illustrated in Fig. 1. A pair of nominally Ohmic contacts on the top surface of the GaAs/AlGaAs heterostructure are connected to a lock-in amplifier that serves to measure the photovoltage, as chopped microwave or terahertz radiation is incident upon the surface of the semiconductor heterostructure. A Schottky barrier occurs near the native top surface of the semiconductor heterostructure as illustrated in the center of Fig. 1. The 2DES typically lies nearly 100 nm below the semiconductor surface, in a triangular well at the buried GaAs/AlGaAs interface. The existence of this Schottky barrier hinders contact formation to the 2DES. To form an Ohmic contact, Au-Ge/Ni or In are deposited and alloyed on the top surface at $\approx$450 °C in a forming gas atmosphere. In the case of Au-Ge/Ni, the alloying dopes the wide-gap AlGaAs layer with Ge, a group-IV element, and reduces the Schottky barrier width, helping to form a nominally Ohmic contact. In the case of In contacts, the alloying helps to form AlInGaAs below the contacts, and this reduces the Schottky barrier height, helping once again to form nominally Ohmic contacts.[68] Although in both cases the contacts are nominally Ohmic, there is often some remnant of the initial nonlinearity in the I-V characteristics of the contacts.

The PV measurement was carried out by chopping the incident microwave radiation at 1 kHz and detecting the resulting voltage at the chop frequency using a lock-in amplifier. For concurrent measurements of R_{xx} and PV, a low-frequency ($\approx$13 Hz) current was applied to the specimen in conjunction with chopped (1 kHz) photoexcitation. A pair

of lock-in amplifiers with appropriately set, nonoverlapping, band-pass filters were then used to concurrently measure the $R_{xx} = V_{xx}/I$ and PV. Although two lock-in amplifiers are employed in such a concurrent measurement, the results do not correspond to a standard double modulation measurement because the output of one lock-in does not become the input to the other lock-in amplifier.

III. RESULTS

Figure 2 exhibits the diagonal resistance, R_{xx}, vs the magnetic field B under (a) 240 GHz, (b) 300 GHz, and (c) 360 GHz photoexcitation. All three panels exhibit strong radiation-induced magnetoresistance oscillations (RIMRO) in R_{xx}, above the 230 GHz quench threshold identified in Ref. 18. Since the characteristic field, $B_f = 2\pi m^* f/e$, for the radiation-induced magnetoresistance oscillations increases linearly with the radiation frequency, f, the slowly-varying-with-B radiation-induced oscillations shift to higher B with increasing f. Note that, at these relatively large f, these radiation-induced oscillations do overlap the more-rapidly-varying-with-B Shubnikov–de Haas (SdH) oscillations; see also Refs. 17, 21, and 22. A close comparison of Figs. 2(a)–2(c) shows that, in the low-B limit, the radiation-induced magnetoresistance oscillations extend below $B = 0.1$ T, to the same low magnetic field threshold. This feature suggests that the broadening is not dependent on the radiation frequency here. However, there is a reduction in the amplitude of the radiation-induced magnetoresistance oscillations for a fixed index oscillatory maximum, especially at 360 GHz. We attribute this feature to an effective decrease in radiation power at the highest f. A more careful analysis leading to the same conclusion follows in Fig. 3.

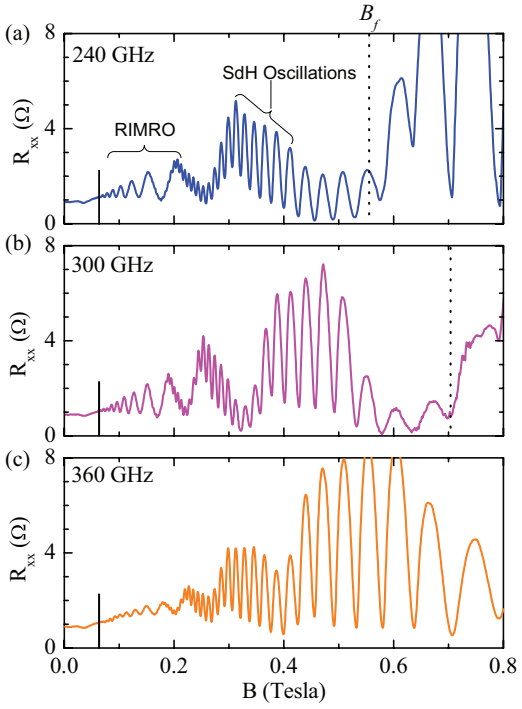

FIG. 2. (Color online) Microwave ($f < 300$ GHz) and terahertz ($f \geqslant 300$ GHz) radiation-induced magnetoresistance oscillations in the diagonal resistance R_{xx}, which overlap Shubnikov–de Haas oscillations, are exhibited for (a) $f = 240$ GHz, (b) $f = 300$ GHz, and (c) $f = 360$ GHz. Here, the slowly varying oscillations are the radiation-induced magnetoresistance oscillations (RIMRO) while the quickly varying oscillations are the Shubnikov–de Haas (SdH) oscillations. A subset of oscillations of each type are marked on the figure. The solid vertical lines below 0.1 T marks the low-B threshold for the appearance of RIMRO. The dotted lines indicate $B_f = 2\pi f m^*/e$ with $m^* = 0.065m$.

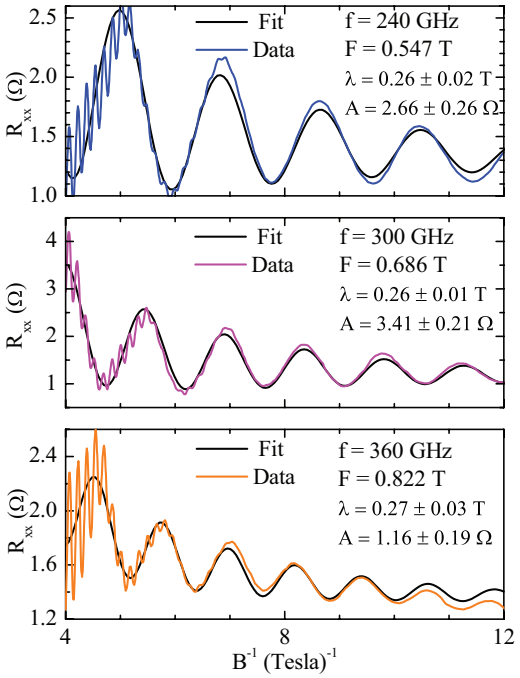

FIG. 3. (Color online) Inverse magnetic field plots of the radiation-induced magneto-resistance oscillations in the diagonal resistance R_{xx} are exhibited for (a) $f = 240$ GHz, (b) $f = 300$ GHz, and (c) $f = 360$ GHz. Also shown are fits to the data using exponentially damped sinusoids, i.e., $\Delta R_{xx} = -A\exp(-\lambda/B)\sin(2\pi F/B)$, with the parameters F,λ and A indicated in the figure. Note that λ is insensitive to the f within experimental uncertainty.

Figure 3 presents inverse-magnetic-field plots of the data of Fig. 2. This figure indicates that the period of the radiation-induced magnetoresistance oscillations is reduced with increasing f, as expected. Also shown in this figure are fits to the oscillatory resistance with exponential damped sinusoids, i.e., $\Delta R_{xx} = -A\exp(-\lambda/B)\sin(2\pi F/B)$.[7,25] Here, the exponential damping can serve to determine a finite frequency broadening lifetime [τ_f] (or single particle lifetime [τ]) and broadening temperature T_f when the exponential damping is written in Dingle form as $\exp(-\lambda/B) = \exp(-\pi/\omega_c\tau_f) \approx \exp(-pT_f/B)$.[7] The fits results, see Fig. 3, indicate that $\lambda \approx 0.26$ T, which corresponds to $T_f \approx 260$ mK, is constant and insensitive to f, within experimental uncertainties. In Ref. 7, λ was shown to be insensitive to f over the band $30 < f < 120$ GHz. Thus, these results suggest similar behavior over the band examined in Fig. 3, to $f = 360$ GHz.

Figure 4 exhibits R_{xx} and the concurrently measured photovoltage (PV) under (a) 42 GHz, (b) 225 GHz, and

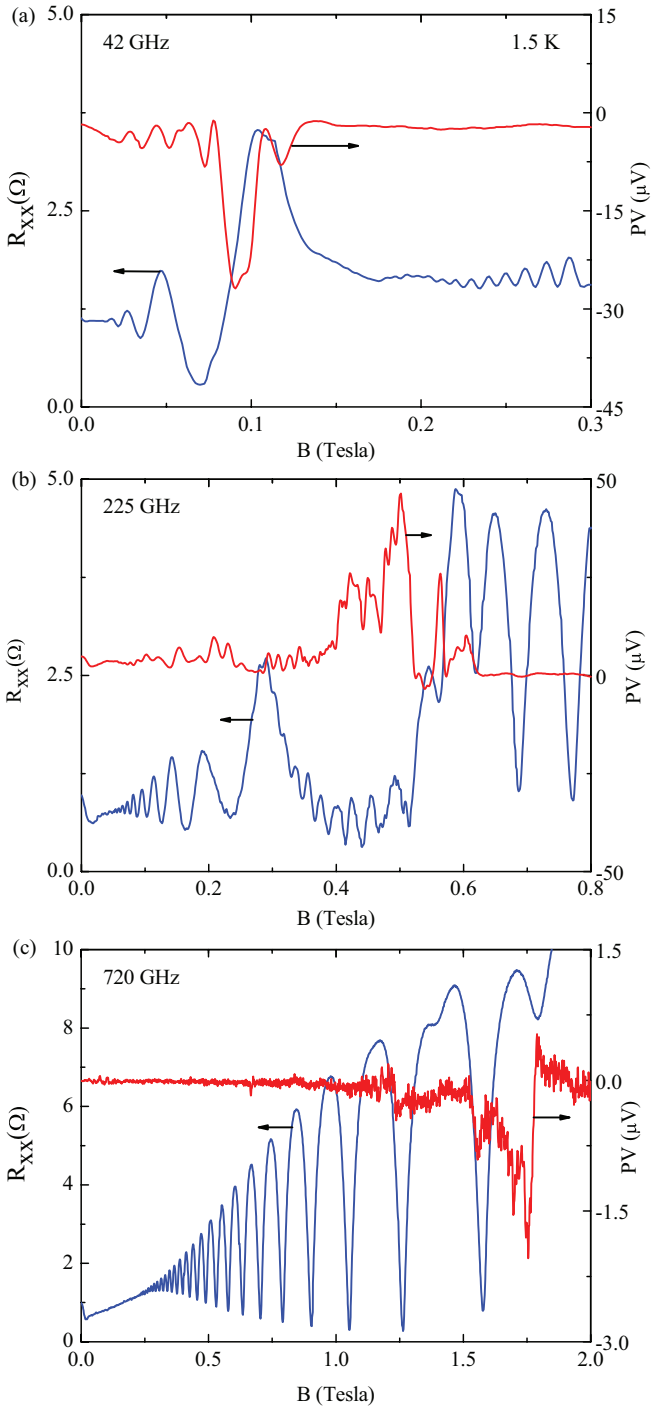

FIG. 4. (Color online) (a) Microwave-induced magnetoresistance oscillations in R_{xx} at $f = 42$ GHz are shown on the left ordinate. The concurrently measured photo-voltage (PV) is shown on the right ordinate. The PV shows a large and broad feature in the vicinity of the node of the R_{xx} oscillations at $B = 0.1T$. (b) R_{xx} (left-ordinate) and PV (right ordinate) at $f = 225$ GHz. (c) R_{xx} (left-ordinate) and PV (right ordinate) at $f = 720$ GHz. The largest features in the PV in panels (a) - (c) are associated with cyclotron resonance.

(c) 720 GHz photoexcitation. Figure 4(a) shows that, at 42 GHz, a broad and deep minimum becomes observable in the PV near the node in the radiation-induced magnetoresistance oscillation at $B \approx 0.1$ T. Figure 4(b) shows that a broad PV maximum, with structure within, becomes observable near the node in the radiation-induced magnetoresistance oscillation at $B \approx 0.525$ T, at $f = 225$ GHz. Figure 4(c) shows an irregular minimum in the PV in the vicinity of 1.75 T. Here, at $f = 720$ GHz, the R_{xx} does not exhibit perceptible radiation-induced magnetoresistance oscillations due to insufficient source power in this f band.

Figure 5 examines the evolution of the PV signal with f over the range $42 \leqslant f \leqslant 720$ GHz for the specimen with In contacts. Here, in Figs. 5(a) and 5(b), the data traces have been offset vertically for the sake of presentation. Figure 5(a) shows that a pronounced, irregularly shaped broad structure in the PV shifts to higher B with increasing f. Figure 5(b) shows the PV signal plotted vs the normalized magnetic field, B/B_f, where $B_f = 2\pi f m^*/e$. This plot shows that the pronounced feature in the PV signal occurs near $B/B_f \approx 1$. An interesting point in Fig. 5(a) [and Fig. 5(b)] is that the PV feature at some f extend above—and at other f extend below—the background value. Note that, since the PV signifies a voltage difference between a pair of contacts, the sign of the PV depends upon the relative electrochemical potentials of the two contacts. This could depend upon the f-dependent profile of the radiation field over the sample, and also the relative quality of the contacts. Nevertheless, we determined the approximate center of the PV feature at each f and also measured the width of the PV feature to obtain an uncertainty estimate of this apparent resonance. The center of the PV feature is symbolized by B_R and plotted vs f on the left ordinate in Fig. 5(c). Here, the error bar associated with each point corresponds to the width estimate of the PV feature mentioned above. Figure 5(c) shows that the B_R increases linearly with f. A linear least-squares fit to the data indicates that $B_R = 2.38 \pm 0.03 \times 10^{-3} f$, where B_R is in units of Teslas and f is in units of GHz.

Figure 6 examines the evolution of the PV signal with f for a 200 μm wide Hall bar specimen with alloyed Au-Ge/Ni contacts over the range $120 \leqslant f \leqslant 725$ GHz. As in Fig. 5, the PV structure in Fig. 6(a) is irregularly shaped, with extensions at resonance both above and below the baseline of the trace, depending upon f. Nevertheless, we once again determined the approximate center of the PV feature at each f and also measured the approximate width of this PV resonance, and plot the results in Fig. 6(b). A best linear fit through the data points of Fig. 6(b) indicates that $B_R = 2.34 \pm 0.04 \times 10^{-3} f$. Note that we obtain consistency in the slope, dB_R/df, of the best-fit lines shown in Figs. 5(c) and 6(b), within experimental uncertainties.

The slopes of the best-fit lines can be understood by attributing the observed PV features to cyclotron resonance. In the GaAs/AlGaAs system, the "standard value" for the electron effective mass is $m^* = 0.067m$, which implies that the cyclotron resonance field depends on the radiation frequency as: $B_C = 2.38 \times 10^{-3} f$, with B_C in units of Teslas and f in units of GHz. A comparison of the results of Figs. 5(c) and 6(b) with these expectations indicates a cyclotron resonance origin for the observed resonant PV feature, i.e., $B_R \approx B_C$. Since the electron effective mass determined from the radiation-induced magnetoresistance oscillations, $m^* = 0.065m$, is known to differ slightly from the standard value, $m^* = 0.067m$ (see Ref. 5), B_f may not be quite the same as B_C.

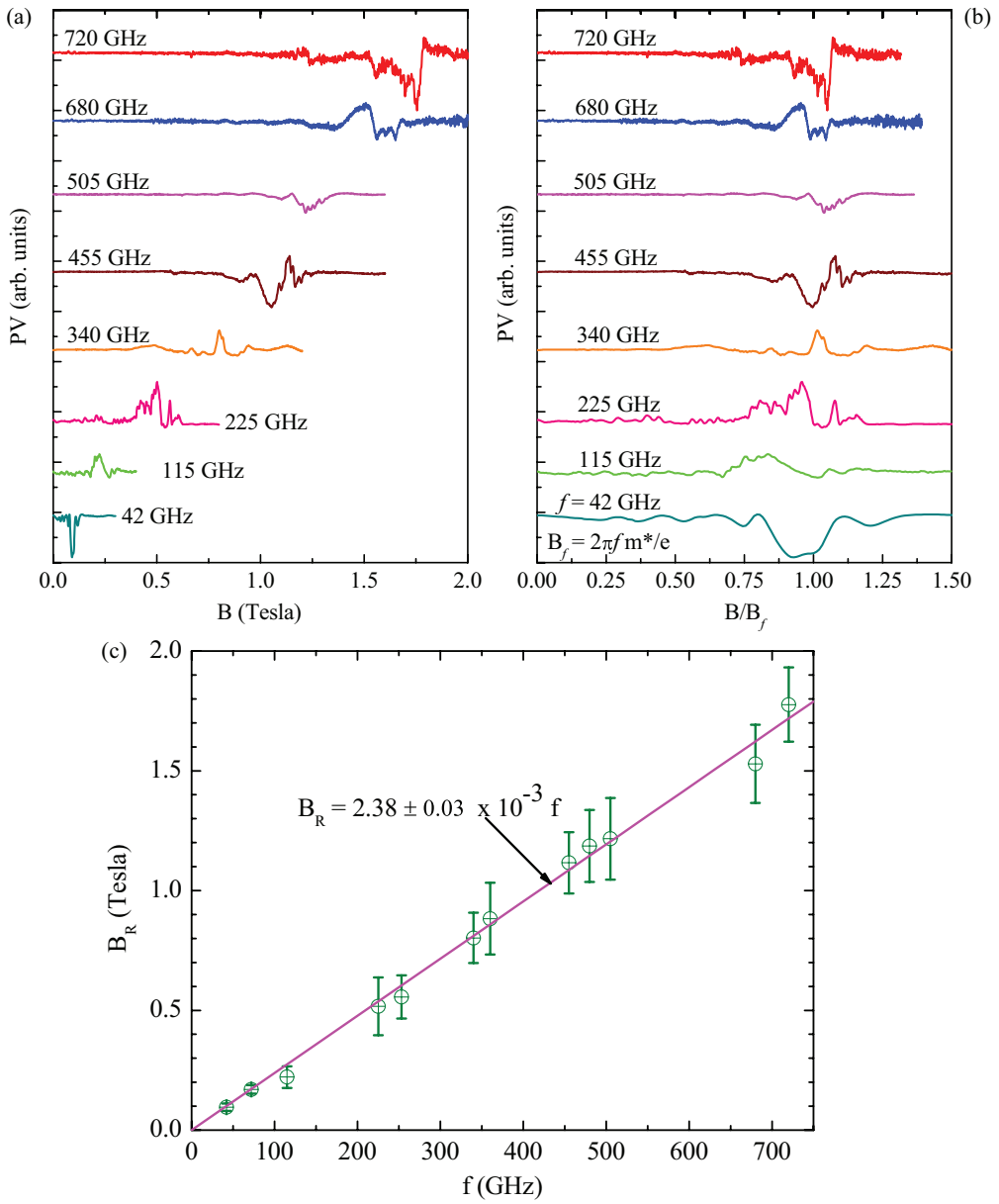

FIG. 5. (Color online) (a) The radiation-induced photo-voltage (PV) is exhibited for a set of excitation frequencies over the range $42 \leqslant f \leqslant 720$ GHz for a specimen with In contacts. Here, the curves have been stacked, i.e., offset vertically, for the sake of presentation. Note the progression of the strong feature in the PV to higher B with increasing f. (b) The radiation-induced photo-voltage (PV) is plotted vs the normalized magnetic field, B/B_f, where $B_f = 2\pi f m^*/e$, with $m^* = 0.065m$; see Ref. 5. Note that the PV structure occurs at similar values of B/B_f at all f. (c) The magnetic field, B_R, of the strong feature in the PV shown above, is plotted vs the radiation frequency, f. A best linear fit, following the equation $B_R = 2.38 \pm 0.03 \times 10^{-3} f$, is shown as the magenta colored line. The error bars associated with the symbols provide a measure of the width of the PV feature along the magnetic field axis in panel (a).

IV. DISCUSSION

The two main results reported here are (a) the observation of radiation-induced magnetoresistance oscillations in R_{xx} above 230 GHz, and (b) the indication of cyclotron resonance in the photovoltage up to 725 GHz.

Point (a) is interesting because, as mentioned, Ref. 18 has argued for the quenching of radiation-induced magnetoresistance oscillations starting at 120 GHz, where the quenching took the form of both a reduction in the amplitude and a decrease in the number of observable oscillations with increasing f. The latter feature was attributed to an apparent increase in the level broadening with the radiation frequency.[18] The results shown here in Fig. 2 indicate observability of the radiation-induced magnetoresistance oscillations in R_{xx} to $f = 360$ GHz. At the highest f, the oscillation amplitude appears reduced due to a drop in the source power. An increase in the Landau level broadening with f is not indicated here since there is no perceptible change in the low field threshold for the observability of the radiation-induced magnetoresistance oscillations with increasing f; see Fig. 2. Further, a lineshape fit indicates no perceptible change in the damping parameter λ,

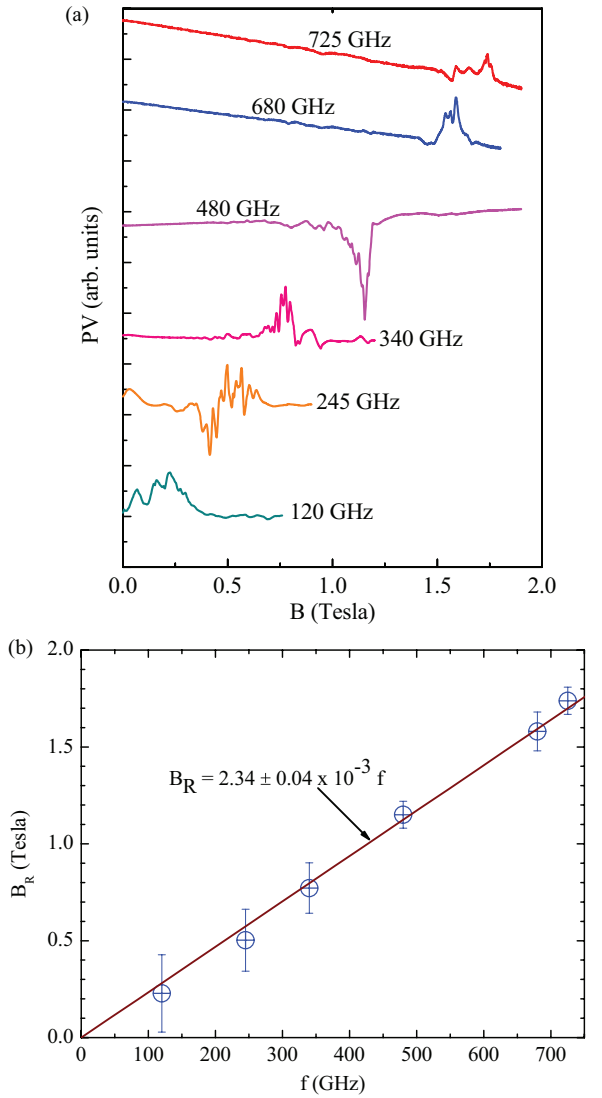

FIG. 6. (Color online) (a) The radiation-induced photo-voltage (PV) is exhibited for a sample with Au-Ge/Ni contacts over the range $120 \leqslant f \leqslant 725$ GHz. Here, the curves have been offset vertically for the sake of presentation. Note the progression of the strong feature in the PV to higher B with increasing f. (b) The magnetic field, B_R, of the PV feature is plotted vs the radiation frequency, f. A best linear fit, following the equation $B_R = 2.34 \pm 0.04 \times 10^{-3} f$, is shown as the magenta colored line. The error bars associated with the symbols provide a measure of the width of the PV feature along the magnetic field axis in panel (a).

and therefore the broadening temperature and/or lifetime, with increasing f, within experimental uncertainties; see Fig. 3. The origin of this difference between our observations and Ref. 18 is not understood at the present. Perhaps, there are some subtle differences in the MBE GaAs/AlGaAs material prepared using different recipes in different laboratories, that are the cause of the observed differences. Although we have reported radiation-induced magnetoresistance oscillations to $f = 360$ GHz, we have not yet succeeded in obtaining strong oscillations at much higher f. There appear to be two reasons for this: (i) Losses between source and sample amount to between 10 to 20 dB at high f, and available radiation sources are simply unable to provide sufficient source power at $f \geqslant 400$ GHz to compensate for the losses. (ii) Our experimental observations suggest that the radiation-induced magnetoresistance oscillations could be sensitive to the photon flux density, i.e., number of photons per unit time per unit area, rather than the incident radiation intensity, i.e., energy per unit time per unit area. According to the displacement model, see, for example, Ref. 34, each photon produces one inter-Landau-level transition, if multiphoton effects are not considered. In this case, the photon flux density could be a critical parameter, and to maintain a constant photon flux density with increasing f, the source intensity would need to increase linearly with f. In such a situation, a factor-of-ten increase in the f from, say, 40 to 400 GHz, would call for a proportionate $10\times$ increase in the source power. Unfortunately, however, in the terahertz regime, source power is more difficult to realize than the microwave regime. Finally, the inelastic model, see Eq. (10) in Ref. 45, predicts that for $\omega_c \ll \omega$, where $\omega = 2\pi f$ and $\omega_c = eB/m^*$, the amplitude of the radiation-induced magnetoresistance oscillations should decrease as $1/\omega^4$.

Simply put, radiation source hardware limitations and inefficient radiation transmission seem to limit, at least in part, the observability of radiation-induced magnetoresistance oscillations at high f.

Point (b)—the observability of cyclotron resonance in the photovoltage to 725 GHz—is remarkable because, unlike traditional cyclotron resonance measurements, this PV measurement does not require a supplemental bolometric detector. Also, this PV measurement of cyclotron resonance utilizes linearly polarized radiation, not the usual circular polarized radiation.

An infinite 2DES is expected to exhibit a plasmon response as $\omega_p^2 = ne^2k/2\epsilon_{\rm eff}\epsilon_0 m^*$, where ω_p is the plasmon frequency, n is the carrier density, e is the electron charge, k is the plasmon wave vector, m^* is the effective mass, and $\epsilon_{\rm eff} = 13.8$.[69] The application of a transverse magnetic field hybridizes cyclotron resonance with the plasmon response, producing the magnetoplasmon response, which follows $\omega_{mp}^2 = \omega_p^2 + \omega_c^2$.[69] In a finite-size specimen, the length scale set by the sample boundary can determine the plasmon (ω_p) response with $k = \pi/W$, where W is the Hall-bar width.[70] For a Hall bar with width $W = 200$ μm, $k = 15.7 \times 10^3$ m^{-1} and $\omega_p = 1.99 \times 10^{10}$ rad/s. At $f = 100$ GHz, $\omega_c = 6.28 \times 10^{11}$ rad/s. Thus, $\omega_c \gg \omega_p$, and therefore $\omega_{mp} \approx \omega_c$ over the f range examined here in the Hall-bar specimen. For this reason, similar results are observed for the cleaved specimen and the Hall bar in Figs. 5(b) and 6(b), respectively.

As mentioned, although the contacts utilized in the PV measurement are nominally Ohmic, there is nonlinearity in the I-V characteristics of the contacts. Photoexcitation of a 2DES with terahertz radiation can produce inter-Landau-level transitions when the radiation energy equals the Landau level spacing in the presence of a perpendicular magnetic field, i.e., $hf = \hbar\omega_c$; see Fig. 1, bottom. Such transitions can change the shape of the self-consistent triangular well by redistributing charge between the Landau levels near the Fermi level. This change in the self-consistent potential well can be propagated through the band structure to the surface, leading to a change in the contact electrochemical potential and a photovoltage

measured across the top-side contacts. An interesting feature in the experimental results is that the sign of the photovoltage in the vicinity of resonance is variable and not amenable to prediction. We attribute this characteristic to the point that the measured PV represents an electrochemical potential difference between two contacts, therefore the sign of the response could change, in principle, if the photoexcitation does not produce precisely the same response in the vicinity of the two contacts. Curiously, such a picture seems to require an inhomogeneity in the contact quality or the radiation intensity across the specimen in order to develop the *voltage difference* between two contacts. The experimental situation suggests, however, that neither of these possibilities can be ruled out at the moment.

V. SUMMARY AND CONCLUSION

An experimental study of the high-mobility GaAs/AlGaAs system indicates strong radiation-induced magnetoresistance oscillations in R_{xx} to nearly 360 GHz. In addition, cyclotron resonance is observed in the photovoltage to 725 GHz. These results show that our high-mobility GaAs/AlGaAs 2DES remains photoactive in magnetotransport into the terahertz band.

ACKNOWLEDGMENTS

Basic research and support for A.N.R. at GSU has been funded by the DOE under Grant No. DE-SC0001762. Terahertz work at GSU has been supported by the Army Research Office under Grant No. W911NF-07-01-015.

[1] R. G. Mani, J. H. Smet, K. von Klitzing, V. Narayanamurti, W. B. Johnson, and V. Umansky, Nature (London) **420**, 646 (2002).
[2] M. A. Zudov, R. R. Du, J. A. Simmons, and J. L. Reno, Phys. Rev. B **64**, 201311 (2001).
[3] P. D. Ye, L. W. Engel, D. C. Tsui, J. A. Simmons, J. R. Wendt, G. A. Vawter, and J. L. Reno, Appl. Phys. Lett. **79**, 2193 (2001).
[4] R. G. Mani, V. Narayanamurti, K. von Klitzing, J. H. Smet, W. B. Johnson, and V. Umansky, Phys. Rev. B **69**, 161306 (2004).
[5] R. G. Mani, J. H. Smet, K. von Klitzing, V. Narayanamurti, W. B. Johnson, and V. Umansky, Phys. Rev. Lett. **92**, 146801 (2004).
[6] R. G. Mani, V. Narayanamurti, K. von Klitzing, J. H. Smet, W. B. Johnson, and V. Umansky, Phys. Rev. B **70**, 155310 (2004).
[7] R. G. Mani, J. H. Smet, K. von Klitzing, V. Narayanamurti, W. B. Johnson, and V. Umansky, Phys. Rev. B **69**, 193304 (2004).
[8] R. G. Mani, Physica E (Amsterdam) **22**, 1 (2004); **25**, 189 (2004); Appl. Phys. Lett. **85**, 4962 (2004).
[9] S. A. Studenikin, M. Potemski, P. T. Coleridge, A. S. Sachrajda, and Z. R. Wasilewski, Solid State Commun. **129**, 341 (2004).
[10] A. E. Kovalev, S. A. Zvyagin, C. R. Bowers, J. L. Reno, and J. A. Simmons, Solid State Commun. **130**, 379 (2004).
[11] R. L. Willett, L. N. Pfeiffer, and K. W. West, Phys. Rev. Lett. **93**, 026804 (2004).
[12] R. R. Du *et al.*, Physica E (Amsterdam) **22**, 7 (2004).
[13] R. G. Mani, IEEE Trans. Nanotechnol. **4**, 27 (2005); Phys. Rev. B **72**, 075327 (2005); Solid State Commun. **144**, 409 (2007); Physica E **40**, 1178 (2008).
[14] B. Simovic, C. Ellenberger, K. Ensslin, H. P. Tranitz, and W. Wegscheider, Phys. Rev. B **71**, 233303 (2005).
[15] J. H. Smet, B. Gorshunov, C. Jiang, L. Pfeiffer, K. West, V. Umansky, M. Dressel, R. Meisels, F. Kuchar, and K. von Klitzing, Phys. Rev. Lett. **95**, 116804 (2005).
[16] Z. Q. Yuan, C. L. Yang, R. R. Du, L. N. Pfeiffer, and K. W. West, Phys. Rev. B **74**, 075313 (2006).
[17] R. G. Mani, Appl. Phys. Lett. **91**, 132103 (2007).
[18] S. A. Studenikin, A. S. Sachrajda, J. A. Gupta, Z. R. Wasilewski, O. M. Fedorych, M. Byszewski, D. K. Maude, M. Potemski, M. Hilke, K. W. West, and L. N. Pfeiffer, Phys. Rev. B **76**, 165321 (2007).
[19] A. Wirthmann, B. D. McCombe, D. Heitmann, S. Holland, K.-J. Friedland, and C.-M. Hu, Phys. Rev. B **76**, 195315 (2007).
[20] S. Wiedmann, G. M. Gusev, O. E. Raichev, T. E. Lamas, A. K. Bakarov, and J. C. Portal, Phys. Rev. B **78**, 121301(R) (2008).
[21] R. G. Mani, Appl. Phys. Lett. **92**, 102107 (2008).
[22] R. G. Mani, W. B. Johnson, V. Umansky, V. Narayanamurti, and K. Ploog, Phys. Rev. B **79**, 205320 (2009).
[23] L. C. Tung, C. L. Yang, D. Smirnov, L. N. Pfeiffer, K. W. West, R. R. Du, and Y. J. Wang, Solid State Commun. **149**, 1531 (2009).
[24] S. Wiedmann, N. C. Mamani, G. M. Gusev, O. E. Raichev, A. K. Bakarov, and J. C. Portal, Phys. Rev. B **80**, 245306 (2009).
[25] R. G. Mani, C. Gerl, S. Schmult, W. Wegscheider, and V. Umansky, Phys. Rev. B **81**, 125320 (2010).
[26] A. N. Ramanayaka, R. G. Mani, and W. Wegscheider, Phys. Rev. B **83**, 165303 (2011).
[27] O. M. Fedorych, M. Potemski, S. A. Studenikin, J. A. Gupta, Z. R. Wasilewski, and I. A. Dmitriev, Phys. Rev. B **81**, 201302 (2010).
[28] I. V. Andreev, V. M. Muravev, I. V. Kukushkin, S. Schmult, and W. Dietsche, Phys. Rev. B **83**, 121308 (2011).
[29] R. G. Mani, A. N. Ramanayaka, and W. Wegscheider, Phys. Rev. B **84**, 085308 (2011).
[30] A. N. Ramanayaka, R. G. Mani, J. Inarrea, and W. Wegscheider, Phys. Rev. B **85**, 205315 (2012).
[31] S. Wiedmann, G. M. Gusev, O. E. Raichev, S. Kramer, A. K. Bakarov, and J. C. Portal, Phys. Rev. B **83**, 195317 (2011).
[32] A. Bogan, A. T. Hatke, S. A. Studenikin, A. Sachrajda, M. A. Zudov, L. N. Pfeiffer, and K. W. West, Phys. Rev. B **86**, 235305 (2012).
[33] R. G. Mani, J. Hankinson, C. Berger, and W. A. de Heer, Nat. Commun. **3**, 996 (2012).
[34] A. C. Durst, S. Sachdev, N. Read, and S. M. Girvin, Phys. Rev. Lett. **91**, 086803 (2003).
[35] A. V. Andreev, I. L. Aleiner, and A. J. Millis, Phys. Rev. Lett. **91**, 056803 (2003).
[36] V. Ryzhii and R. Suris, J. Phys.: Condens. Matter **15**, 6855 (2003).
[37] V. Ryzhii and A. Satou, J. Phys. Soc. Jpn. **72**, 2718 (2003).
[38] A. A. Koulakov and M. E. Raikh, Phys. Rev. B **68**, 115324 (2003).
[39] X. L. Lei and S. Y. Liu, Phys. Rev. Lett. **91**, 226805 (2003).
[40] P. H. Rivera and P. A. Schulz, Phys. Rev. B **70**, 075314 (2004).
[41] X. L. Lei, J. Phys.: Condens. Matter **16**, 4045 (2004).
[42] S. A. Mikhailov, Phys. Rev. B **70**, 165311 (2004).
[43] J. Inarrea and G. Platero, Phys. Rev. B **72**, 193414 (2005).
[44] X. L. Lei and S. Y. Liu, Phys. Rev. B **72**, 075345 (2005).
[45] I. A. Dmitriev, M. G. Vavilov, I. L. Aleiner, A. D. Mirlin, and D. G. Polyakov, Phys. Rev. B **71**, 115316 (2005).
[46] J. Inarrea and G. Platero, Phys. Rev. Lett. **94**, 016806 (2005).

[47]A. Auerbach, I. Finkler, B. I. Halperin, and A. Yacoby, Phys. Rev. Lett. **94**, 196801 (2005).
[48]J. Inarrea and G. Platero, Appl. Phys. Lett. **89**, 052109 (2006); **90**, 172118 (2007); **92**, 192113 (2008).
[49]J. Inarrea and G. Platero, Phys. Rev. B **76**, 073311 (2007); **78**, 193310 (2008).
[50]A. D. Chepelianskii, A. Pikovsky, and D. L. Shepelyansky, Eur. Phys. J. B **60**, 225 (2007).
[51]A. Auerbach and G. V. Pai, Phys. Rev. B **76**, 205318 (2007).
[52]I. A. Dmitriev, A. D. Mirlin, and D. G. Polyakov, Phys. Rev. B **75**, 245320 (2007).
[53]P. H. Rivera, A. L. C. Pereira, and P. A. Schulz, Phys. Rev. B **79**, 205406 (2009).
[54]I. G. Finkler and B. I. Halperin, Phys. Rev. B **79**, 085315 (2009).
[55]X. L. Lei and S. Y. Liu, Appl. Phys. Lett. **94**, 232107 (2009).
[56]A. D. Chepelianskii and D. L. Shepelyansky, Phys. Rev. B **80**, 241308(R) (2009).
[57]I. A. Dmitriev, M. Khodas, A. D. Mirlin, D. G. Polyakov, and M. G. Vavilov, Phys. Rev. B **80**, 165327 (2009).
[58]T. Toyoda, Mod. Phys. Lett. B **24**, 1923 (2010).
[59]D. Hagenmuller, S. De Liberato, and C. Ciuti, Phys. Rev. B **81**, 235303 (2010).
[60]J. Inarrea, R. G. Mani, and W. Wegscheider, Phys. Rev. B **82**, 205321 (2010).
[61]J. Inarrea, Appl. Phys. Lett. **100**, 242103 (2012).
[62]X. L. Lei and S. Y. Liu, Phys. Rev. B **86**, 205303 (2012).
[63]P. H. Siegel, IEEE Trans. Microwave Theory Technol. **50**, 910 (2002).
[64]T. G. Phillips and J. Keene, Proc. IEEE **80**, 1662 (1992).
[65]B. B. Hu and M. C. Nuss, Opt. Lett. **20**, 1716 (1999).
[66]R. H. Jacobsen, D. M. Mittleman, and M. C. Nuss, Opt. Lett. **21**, 2011 (1996).
[67]Virginia Diodes, Inc., 979 Second Street S.E., Suite 309, Charlottesville, VA 22902; www.vadiodes.com
[68]R. G. Mani, L. Ghenim, and T. N. Theis, Phys. Rev. B **45**, 12098 (1992); L. Ghenim and R. G. Mani, Appl. Phys. Lett. **60**, 2391 (1992).
[69]D. Heitmann, Surf. Sci. **170**, 332 (1986).
[70]E. Vasiliadou, G. Muller, D. Heitmann, D. Weiss, K. v. Klitzing, H. Nickel, W. Schlapp, and R. Losch, Phys. Rev. B **48**, 17145 (1993).